Review

Key Technologies for the Development of an Automotive MEMS Sensor

Teruhisa Akashi, Motohiro Fujiyoshi, Yoshiyuki Hata, Yutaka Nonomura, Hirofumi Funabashi and Yoshiteru Omura

Report received on Jul. 23, 2012

ABSTRACT The present paper describes three types of elemental technologies for the development of an automotive micro-electro-mechanical-systems (MEMS) sensor. The first technology is extremely deep silicon etching (EDSE) for fabricating a sensor element. The EDSE using a fan-shaped compensation mask pattern has been developed to fabricate a complicated and extremely thick structure composed of different gap widths. The pattern allowed the formation of a 300-μm-thick sense-comb structure without a bridge-shaped silicon residue. The second technology is a *z*-directional anti-stiction technology related to the reliability of the sensor. For preventing a silicon-on-insulator-MEMS (SOI-MEMS) structure that is movable in the *z* direction from sticking to a substrate, a convex poly-Si structure referred to as a poly-Si mushroom-shaped structure (pSiMS) has been developed. A fabricated pSiMS with a height of 0.6 μm prevented 2-mm-long beams from sticking. The final technology is a high-resolution (HR) package leak test, which is related to the long-term reliability of the sensor. A developed chilling HR method detected an extremely low leak rate of 1×10^{-17} Pa·m^3/s, which is 10^5 times superior to the resolution of a conventional method. These technologies support the development of the MEMS sensor.

KEYWORDS Extremely Deep Silicon Etching, Compensation Mask, Poly-Si Mushroom-shaped Structure, *Z*-directional Stiction, Package Leak Test, MEMS

1. Introduction

Automobiles are a major application of micro-electro-mechanical systems (MEMS). A number of MEMS sensors have been used to improve safety during driving. Recently, vehicle stability control (VSC) systems,[1] which are an electronic systems designed to help drivers maintain vehicle control under adverse conditions, have been widely used as a synonym of safety, regardless of the vehicle type. In addition, VSC is becoming standardized for vehicle dynamics control on skiddy and tightly winding roads. The VSC system is composed primarily of an accelerometer and an angular rate sensor, which is a key device in this system. To detect skidding and reduce loss of traction of the vehicle, the sensors detect the in-plane two-axis acceleration and yaw rate. These sensors are usually fabricated by MEMS fabrication technologies.

Recently, deep reactive ion etching (DRIE)[2] of silicon was developed to realize a complicated and high-aspect-ratio structure, independently of a crystal orientation. Before the development of the DRIE, anisotropic wet etching of silicon using alkali solutions such as KOH (potassium hydroxide) and TMAH (tetramethylammonium hydroxide)[3-5] was the primary fabrication technique for silicon bulk micromachining. Anisotropic wet etching is dependent on the crystal orientation.[3] Therefore, a structure fabricated by anisotropic wet etching is limited, and complicated structures, such as a comb drive, a sense comb, and a high-aspect-ratio trench, cannot be formed. Since DRIE is a fabrication process that is independent of the crystal orientation, DRIE has allowed fabrication of more complicated and higher-aspect-ratio structures.

On the other hand, an automotive sensor is required to have high reliability, i.e., long-term reliability, compared with consumer applications. Regarding the MEMS sensor for use in an automobile, high reliability is also required. Therefore, a reasonable solution is to fabricate a structure for ensuring its reliability on a sensor element. Based on this consideration, we focus on the development of not only a device but also an elemental technology in an attempt to realize a MEMS sensor with high reliability.

The present paper reports three elemental technologies that have recently been developed for a capacitive MEMS sensor for use in an automobile. The first technology is extremely deep silicon etching

(EDSE), which is an advanced dry etching technology using a compensation mask pattern. The second technology is an anti-stiction technology used for a silicon-on-insulator-MEMS (SOI-MEMS) structure that is movable in the *z* direction. The third technology is a package leak-test method that is capable of detecting an extremely low leak rate, which can be used for vacuum hermetic packaging. The second and third technologies are related to the reliability of the sensor. These three types of key technologies supporting the development of the capacitive MEMS sensor are discussed herein.

2. Extremely Deep Silicon Etching Technology for Fabricating Thicker Silicon Structures

2. 1 Challenge to Fabricate an Extremely Thick Comb Structure

A comb electrode is generally used for a capacitive MEMS sensor, such as an accelerometer or an angular rate sensor. In particular, a sense-comb electrode is composed of narrow and wide trenches and has different gap widths. To improve the sensor sensitivity, a thicker sense-comb structure is required. DRIE based on the Bosch process[(2)] is usually used for fabricating a high-aspect-ratio or thick structure. However, the fabrication of a sense-comb structure of more than 200 µm in thickness has been quite difficult due to the aspect-ratio-dependent etching (ARDE) problem,[(6)] which induces different etching rates depending on the aspect ratio. This problem induces incomplete etching on the bottom of the trench primarily because the structure consists of narrow and wide trenches. There have been no practical approaches by which to investigate why an extremely thick sense-comb structure is not formed.

2. 2 Bridge-shaped Silicon Residue

Figure 1(a) shows a sense-comb mask pattern for checking an etched profile. The pattern consists of three kinds of gaps: narrow-comb gaps, wide-comb gaps, and tip gaps. Figure 1(b) illustrates a cross-sectional diagram of a sense-comb structure after DRIE. Non-doped silicate glass (NSG) was used as a mask material. To prevent notch formation,[(7)] an etching stop layer of Al-Si-Cu was formed on the backside of a wafer. After DRIE, the Al-Si-Cu layer was removed to observe the profile from the bottom.

Incomplete etching of a sense-comb test pattern was observed. **Figure 2**(a) shows an SEM image of the bottom of the etched sense-comb structure composed of a 15-µm-wide narrow-comb gap, a 45-µm-wide wide-comb gap, and a 10-µm-wide tip gap. The combs were 150 µm in length and 300 µm in thickness. DRIE with 50% over-etching was carried out in order to form the structure with a gap width of 10 µm. However, the 10-µm-wide tip gaps were not completely etched, as shown in Fig. 2(a). Bridge-shaped silicon residues (bridges) were formed on the comb tips. Figure 2(b) shows a cross-sectional SEM image of the structure cleaved along line A-A' in Fig. 2(a). The bridges appeared at depths greater than 200 µm. Moreover, vertical stripes were generated on the trench sidewalls at depths in the range of 150 to 300 µm. The cross-sectional profile of the bridge was almost triangular. The side facing the wide-comb gap was inclined, whereas the side facing the narrow-comb gap was almost vertical. Thus, the bridge was demonstrated experimentally to prevent complete etching.

Figure 3(a) shows bottom views of the fabricated sense-comb structures. All of the structures were etched by DRIE at the same time. In this case, the width of a tip gap ranged from 10 to 40 µm, while the other conditions were fixed. In this figure, Br_1 and Br_2

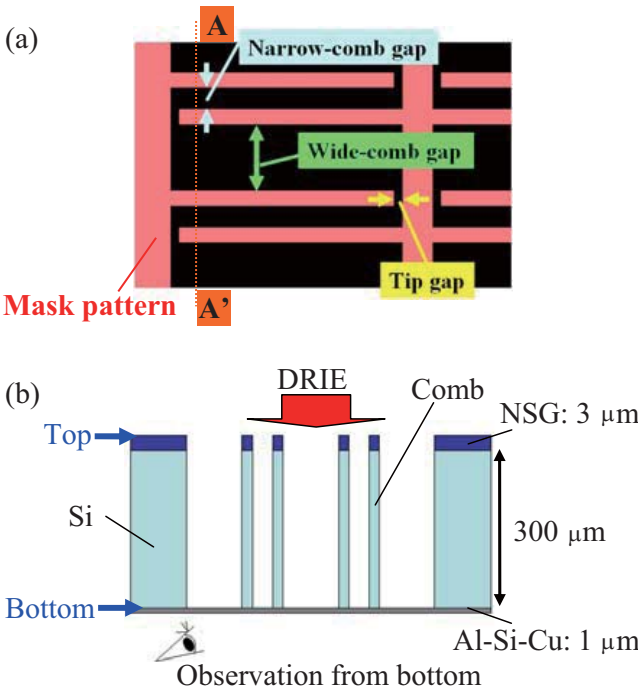

Fig. 1 Sense-comb test structure: (a) mask pattern and (b) A-A' cross-sectional diagram of a sense-comb structure.

indicate the two types of bridges. Bridge Br_1 appeared at the tip gap, and bridge Br_2 appeared at the narrow-comb gap. As the tip gap increased, bridge Br_1 disappeared. In contrast, bridge Br_2 appeared on the 15-μm-wide narrow-comb gap. These results indicate that bridge formation is not avoided by widening the tip gap. Next, Fig. 3(b) shows bottom views of the sense-comb structures composed of wide-comb gaps ranging from 18 to 45 μm. A tight bridge Br_1 was obviously formed as the wide-comb gap increased.

The above-mentioned results demonstrated that the bridge is not formed due to lack of etching time. The bridge appears at the interface where the gap width changes remarkably. When the tip gap is widened, there is a remarkable change in the gap width at the interface between the tip gap and the narrow-comb gap. This interface corresponds to the appearing point of bridge Br_2. When the wide-comb gap is widened, there is a remarkable change in the gap width at the interface between the tip gap and the wide-comb gap. This interface corresponds to the appearing point of bridge Br_1. From this point of view, the position at which the bridge appears can be estimated.

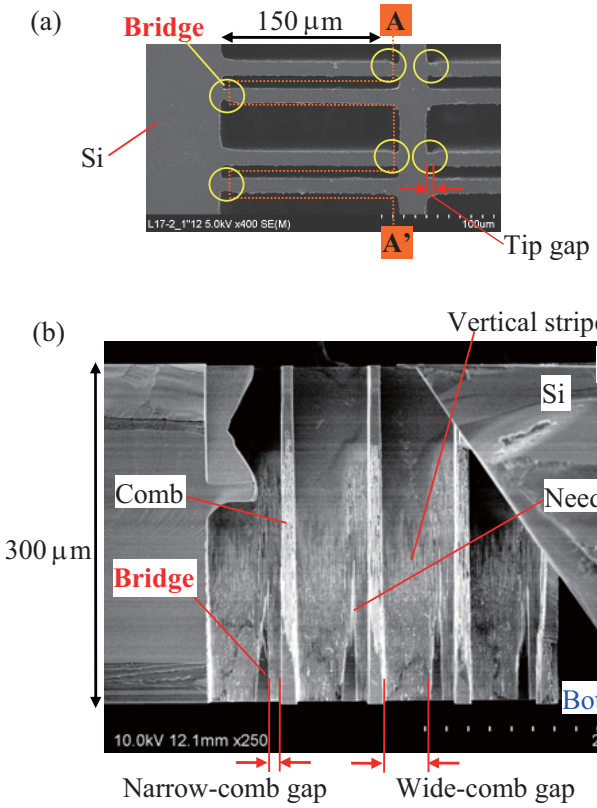

Fig. 2 SEM images of a sense-comb structure and bridge formation: (a) bottom view and (b) A-A' cross-sectional view along the dotted line shown in (a).

2. 3 Mechanism for Generating the Bridge

Based on the DRIE process and the bridge formation characteristics observed in Fig. 3, the mechanism for generating the bridge was derived as follows. **Figure 4** illustrates the steps of the DRIE process to form a sense-comb structure. In step (a), etching progresses uniformly at the beginning of DRIE. In step (b), as the DRIE process progresses further, different etching rates are generated due to the ARDE.[6] As a result, a trench with a narrow gap becomes shallower than a trench with a wide gap. The difference in the etching rate produces a slope. The slope is formed at the interface between a wide tip gap and a narrow-comb gap, as shown on the left of Fig. 4(b). In contrast, the slope is formed at the interface between a wide-comb gap and a narrow tip gap, as shown on the right of Fig. 4(b). In step (c), as the DRIE proceeds further, the slopes become steeper due to the ARDE. In the DRIE process, the passivation film protects the sidewall as well as the bottom of a trench. In addition, ions for subsequent etching attack and remove the passivation film formed on the bottom. In this case, the passivation film on the sidewall is not removed so that the sidewall is protected against etching. Accordingly, the passivation film on the slopes is not completely removed, i.e., the slopes are not completely etched. As the slopes become steeper, the steeper slopes appear to form a wall, which is strongly protected against etching. Finally, in step (d), the slopes are not

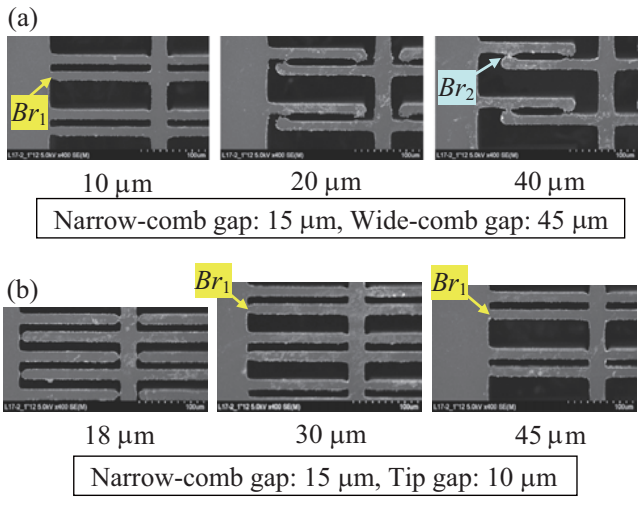

Fig. 3 Bottom views of fabricated sense-comb structures: (a) when the tip gap is changed and (b) when the wide-comb gap is changed.

completely etched even when sufficient over-etching time is spent.

2. 4 Compensation Mask Pattern for EDSE

The sense-comb structure is composed of three types of gaps, as shown in Fig. 1, in order to effectively detect a capacitance change. This means that the structure has different gap widths. Therefore, the structure obviously has a remarkable change in gap width. This remarkable change causes bridge formation, as shown in Fig. 3. To prevent the bridge formation, a compensation mask pattern for EDSE is proposed. **Figure 5** shows a sense-comb mask pattern with the compensation pattern. A fan-shaped pattern with a radius of R is added to the comb tips, which enables a gradual change to be provided in the gap width.

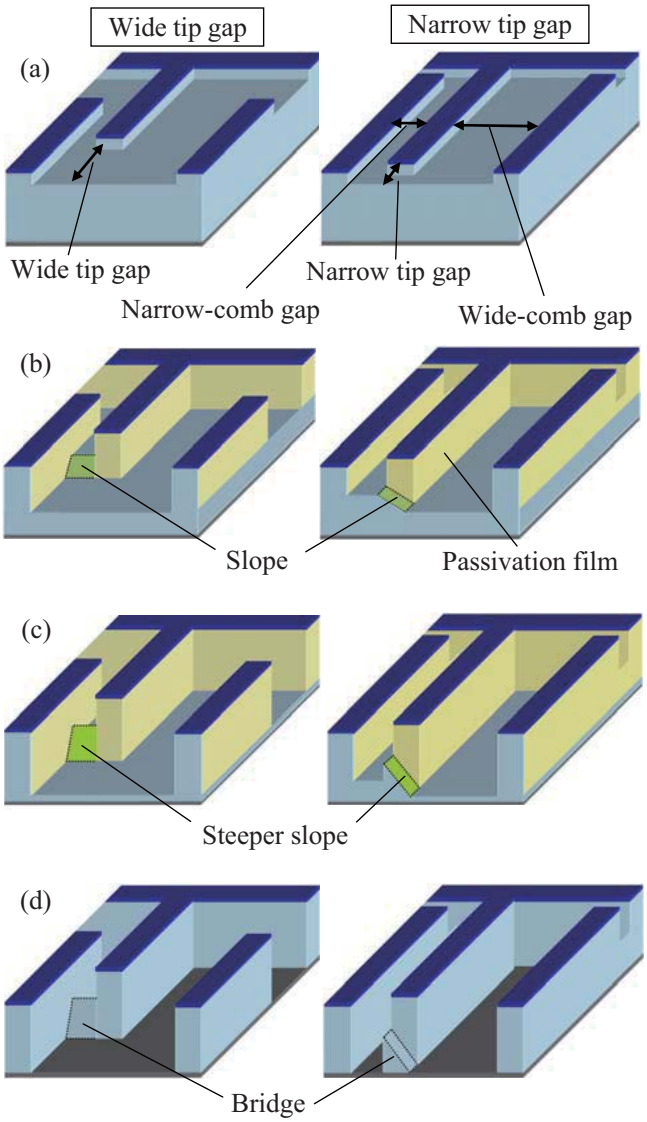

Fig. 4 DRIE process steps for explaining the mechanism for generating the bridge: (a) initial step of DRIE, (b) slope formation with ARDE, (c) steeper slope formation, and (d) bridge formation.

Figure 6 shows SEM images of fabricated 300-μm-thick sense-comb structures without and with the compensation patterns. In this case, the width of the tip was 15 μm, which is equal to that of a narrow-comb gap, in order to avoid a remarkable width change at the interface between the tip gap and the narrow-comb gap. Here, the radius of the fan-shaped pattern was 25 μm. The structures without and with the compensation patterns were fabricated under the same etching time. Without the pattern, bridge Br_1 was formed, whereas with the pattern, bridge Br_1 was not formed. The fan-shaped compensation-mask pattern

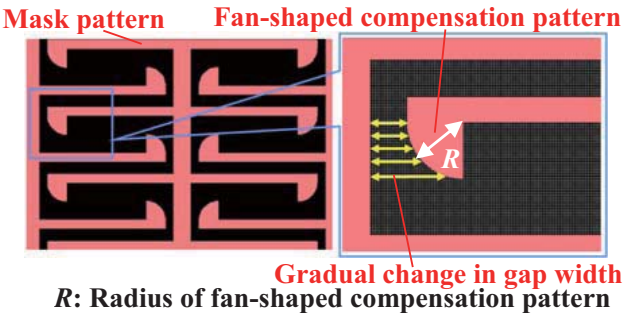

Fig. 5 Compensation mask pattern for a sense-comb structure.

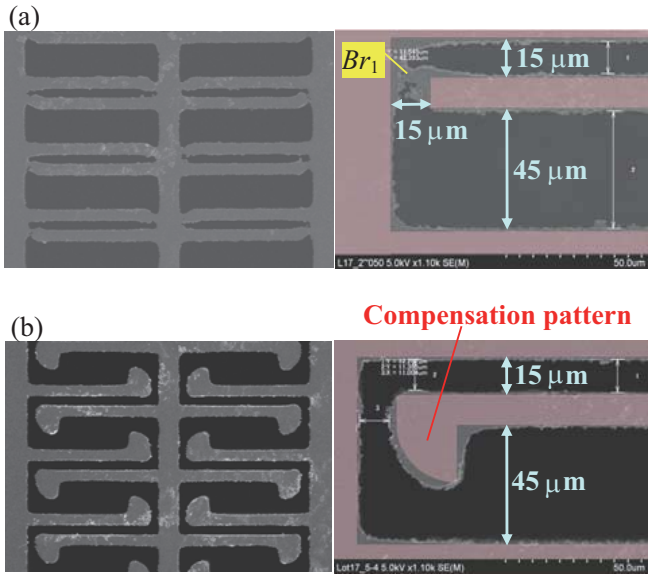

Fig. 6 Bottom views of fabricated sense-comb structures: (a) without and (b) with compensation mask patterns. The shadows indicate the mask patterns.

for the EDSE prevented bridge formation, even though the same etching conditions were applied, which allows a 300-µm-thick sense-comb structure to be fabricated. Accordingly, the proposed compensation pattern is required to form an extremely thick structure composed of different gap widths.

3. *Z*-directional Anti-stiction Technology for Ensuring High Reliability

3. 1 Improvement in Reliability of a Sensor Element

A capacitive MEMS sensor is usually fabricated on an SOI wafer. Such a sensor element has a movable structure. The movable SOI-MEMS structure frequently sticks to the substrate. Such stiction is a fatal flaw, so that preventing stiction is highly desirable for improving the sensor reliability.

Van der Waals forces, hydrogen bridges, and electrostatic forces are considered to cause stiction after the movable structure is brought into physical contact with the substrate.[8] Typically, *z*-directional stiction occurs when there is a gap of a few microns between the movable structure and the substrate. For preventing *x*- and *y*-directional stiction, a stopper on the SOI-MEMS structure is usually fabricated. However, due to the substrate configuration, it is not possible to form a *z*-directional stopper on the movable SOI-MEMS structure. Therefore, a novel convex poly-Si stopper structure for a movable SOI-MEMS structure is proposed for a *z*-directional anti-stiction technology.

3. 2 Mushroom-shaped Convex Poly-Si Structure

Figure 7 shows doubly clamped beams on which convex poly-Si structures are formed. The structure is referred to as a poly-Si mushroom-shaped structure (pSiMS) because the structure has a convex shape that resembles the pileus of a mushroom. The pSiMS is composed of a stipe and a pileus. The pSiMS is firmly fixed to the beam due to the stipe formation. In addition, the pSiMS is effective at reducing the contact area due to the rounded convex shape. This means that the pSiMS can prevent stiction due to the small contact area. Furthermore, if the pileus height is much smaller than a gap corresponding to the thickness of a SiO_2 layer, the pSiMS has no influence on the capacitive sensor performance.

To evaluate the effectiveness of the pSiMS, cantilever and doubly clamped beams with and without the pSiMS were designed. The beam width and thickness were 30 and 15 µm, respectively. The maximum beam length was set to be 2,000 µm. The beam length started from 100 µm and increased by increments of 5 µm. For the pSiMS design, the pileus shape was set to be 0.6 µm in height and 2.7 µm in diameter, and the diameter of the stipe was set to be 1.5 µm.

3. 3 Fabrication

The process flow for a movable structure on which pSiMSs are formed is shown in **Fig. 8**. The starting material was a (100)-oriented SOI wafer composed of a 15-µm-thick top silicon layer, a 3-µm-thick buried oxide layer, and a 300-µm-thick bottom silicon layer. The process consists primarily of two steps: (1) the formation of a mold and (2) refilling of the mold with poly-Si.

In step (a), non-doped silicate glass (NSG) and silicon nitride (SiN) films were deposited. Circular resist mask patterns with a diameter of 1.5 µm were formed, and their films were etched by reactive ion etching (RIE). After that, through-holes were formed by DRIE. In step (b), the resist was removed, and an oxide layer was etched isotropically by a buffered HF (BHF) solution containing a surfactant. The depth of the etched grooves was controlled to be 0.6 µm. The through-holes and the etched grooves formed molds.

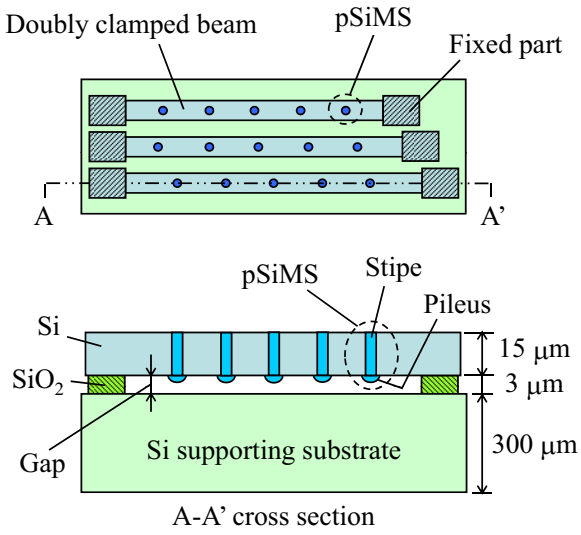

Fig. 7 Doubly clamped beams on which poly-Si mushroom-shaped structures (pSiMSs) are formed.

In step (c), a poly-Si film was deposited by low-pressure chemical vapor deposition (LPCVD). The molds were refilled with poly-Si. In step (d), the poly-Si, SiN, and NSG films were removed. In step (e), a resist mask pattern of beam structures was formed. The beam structures were fabricated by the DRIE. In step (f), the resist mask was removed, and the beam structures were released by HF vapor etching. The movable beam structures with the pSiMSs were fabricated based on this process sequence.

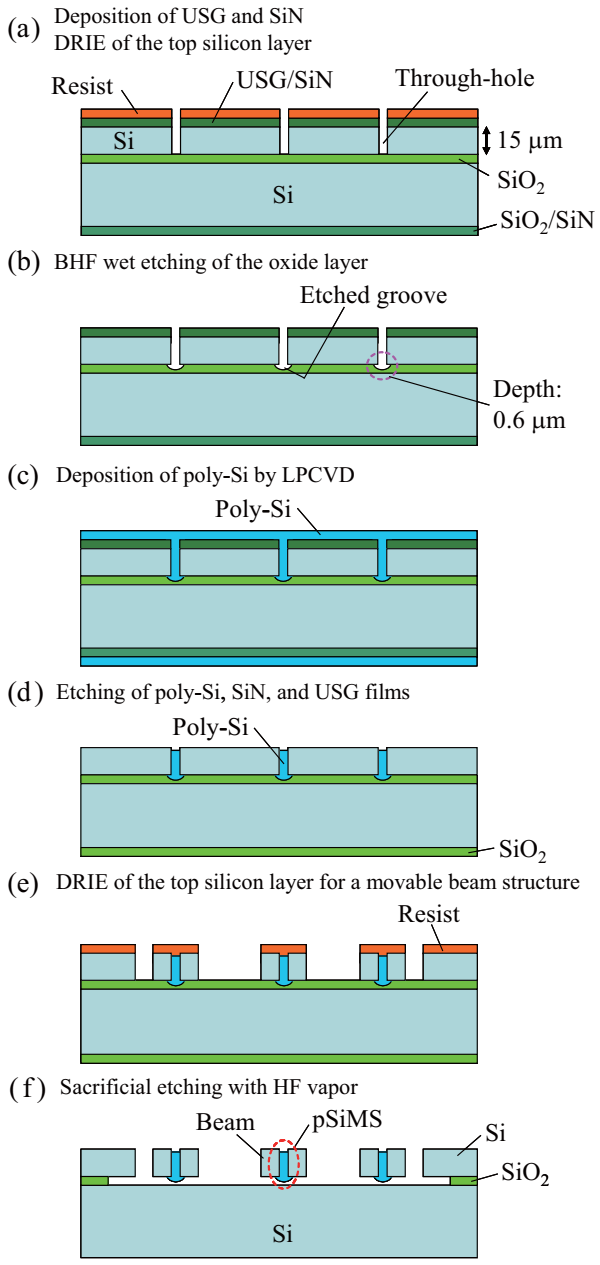

Fig. 8 Fabrication process flow for movable structures with pSiMSs.

3. 4 Experimental Results

Figures 9(a) and (b) show cross-sectional views of a fabricated mold and a mold refilled with poly-Si, respectively. The mold was successfully refilled with poly-Si without the formation of voids or cracks. Moreover, **Fig. 10** shows a pSiMS fabricated on the back side of the beam. Its height was 0.6 μm and its diameter was 2.8 μm. There were no voids or cracks on the surface of the pSiMS. The observed flat surface, with a diameter of 1.58 μm, corresponded to the diameter of the through-hole because the etched groove was fabricated by isotropic wet etching.

To evaluate the effectiveness of the pSiMS, a stiction test was performed by dipping beams into deionized water and then drying the beams in the atmosphere. This test allows the beams to bend and touch the substrate through capillary force. The detachment lengths between the beams with and without the pSiMS were compared.

The left side of **Fig. 11** indicates the measured deformation of the cantilever beams without the pSiMSs, which ranged from 340 to 390 μm in beam

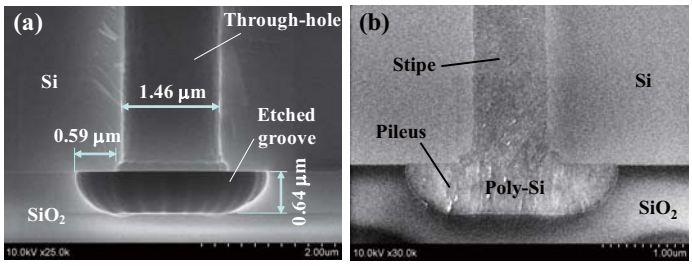

Fig. 9 Cross-sectional views of a fabricated mold: (a) before refilling with poly-Si, (b) after refilling with poly-Si.

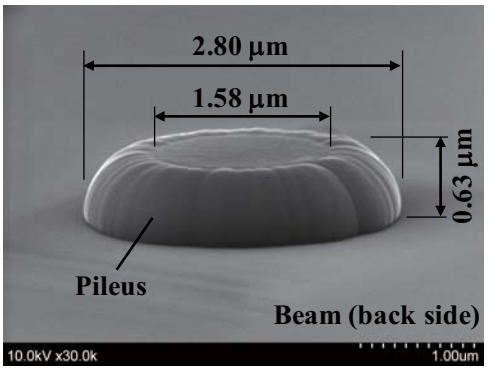

Fig. 10 SEM image of a pSiMS fabricated on the beam.

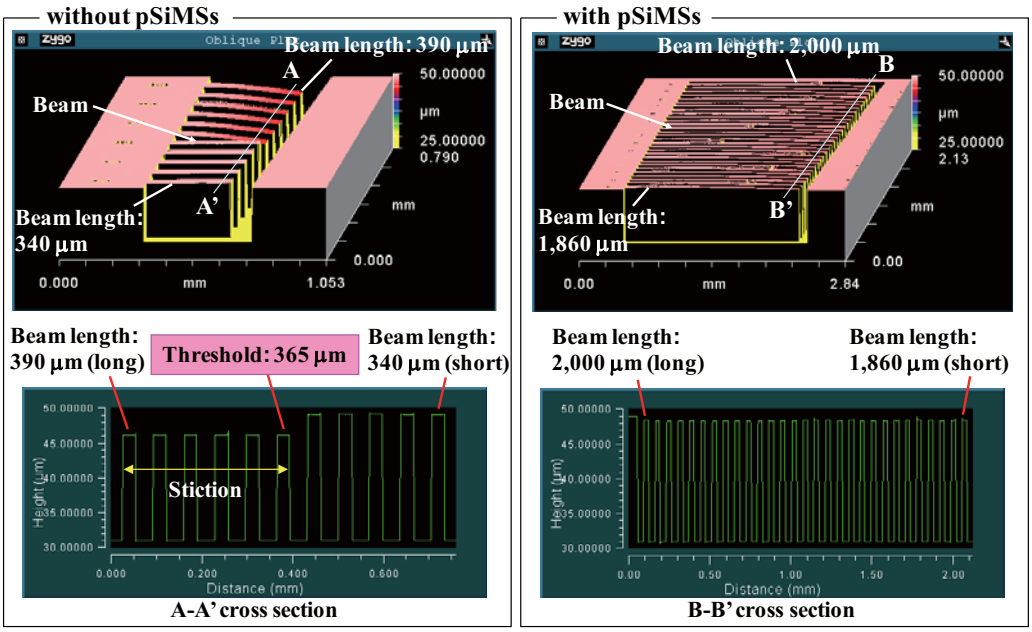

Fig. 11 Deformation of cantilever beams after the stiction test: (a) without pSiMSs and (b) with pSiMSs.

length. Without pSiMSs, the beams that were no less than 365 µm in length stuck. In the case of the cantilever beam, the detachment length was 360 µm, which was similar to the analyzed length of 349 µm. The analyzed length was calculated based on the equation conducted by Mastrangelo and Hsu.[9] In contrast, none of the cantilever beams with pSiMSs stuck, as shown on the right in Fig. 11. In addition, none of the doubly clamped beams with the pSiMSs also stuck. The proposed pSiMSs allowed preventing 2-mm-long beams from sticking. It was confirmed experimentally that the pSiMS is effective for preventing *z*-directional stiction.

4. High-resolution Leak-test Method for a Vacuum Hermetic Package

4. 1 High-resolution Vacuum Integration Method

An angular rate capacitive sensor is usually housed in a vacuum package because a quality factor corresponding to a damping factor related to an air-viscous effect has a significant influence on the sensitivity of the sensor.[10] If a tiny leak is present in the package, then the sensitivity will be degraded gradually. To maintain the sensitivity over the long term, e.g., 15 years, it is important to develop not only a vacuum hermetic packaging technique but also a high-resolution leak-test technique. A helium vacuum integration method has been used as a high-sensitivity, high-resolution method, which indicates a leak-rate resolution of 10^{-12} Pa·m^3/s.[11] However, this value is larger than the resolution necessary to ensure the sensor sensitivity for 15 years. Accordingly, a novel package leak-test method capable of measuring a very tiny leak rate is proposed.

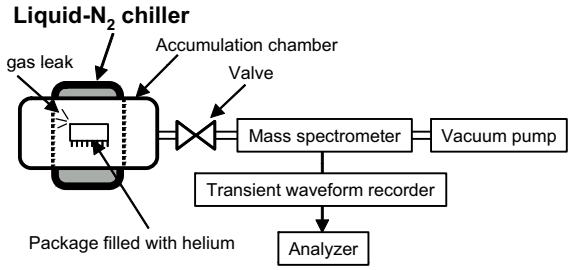

Fig. 12 Configuration of the HR-method measurement system with a liquid-N_2 chiller.

Figure 12 illustrates a high-resolution vacuum-integration-method (HR-method) measurement system with a liquid-nitrogen (LN_2) chiller. The system consists of an accumulation chamber with the chiller, a mass spectrometer, a vacuum pump, a transient waveform recorder, and an analyzer. A leak test using the HR-method system was performed as follows. First, a package filled with helium gas was placed in the chamber. Next, the chamber was evacuated, and the valve connected to the spectrometer was closed.

Then, the gas leaking out of the package was accumulated over the accumulation time t_s. Subsequently, the chamber was chilled by the chiller for reducing background gases. The chilling time was set to be two minutes, based on the experimental results of pressure measurement in the chamber. Before opening the valve, data acquisition was started. The accumulated helium gas was transported to the spectrometer by opening the valve. Finally, the data was acquired and analyzed.

The amount of the helium gas from the chamber was monitored using the spectrometer and was recorded as a transient waveform, as shown in **Fig. 13**. Here, the total amount of helium gas accumulated in the chamber is given as area S. The leak rate Q of the package can be obtained by dividing the total amount of helium gas S by the accumulation time t_s. The advantage of the HR method over the conventional method is high sensitivity and high resolution because leaking helium gas is accumulated for a long time.

4. 2 Experimental Results

Figure 14 shows two transient waveforms, which are output from a mass-spectrometer after opening a valve. Waveform (A) was recorded based on a HR method without an LN_2 chiller (basic HR method) and waveform (B) was recorded based on a HR method with an LN_2 chiller (chilling HR method). Each waveform had a maximum value just after opening the valve. In these cases, there was no helium gas in the accumulation chamber. Therefore, the shaded areas indicate background gases. The shaded area of waveform (B) was quite small compared with that of waveform (A), which indicates that the chilling HR method helps to reduce the background gases.

Figure 15 shows the mass-spectrometer output as a function of accumulation time under different conditions. The basic HR method (A), the chilling HR method (B), and the chilling HR method with baking (C) were compared. Baking was carried out at 150ºC for 120 minutes. In these experiments, there were no packages in the chamber. Therefore, the obtained leak rate, which corresponds to the slope of the regression line, indicates the leak-rate resolution. The resolutions of methods (A), (B), and (C) are 1×10^{-15}, 4×10^{-17}, and 1×10^{-17} Pa·m^3/s, respectively. The leak-rate resolution of method (A) is 10^3 times superior to the

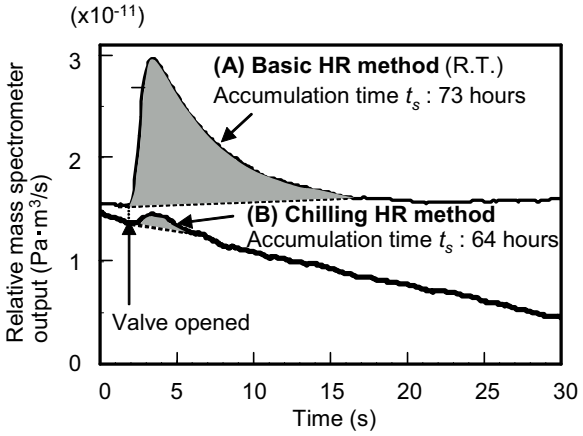

Fig. 14 Transient waveforms of mass-spectrometer output.

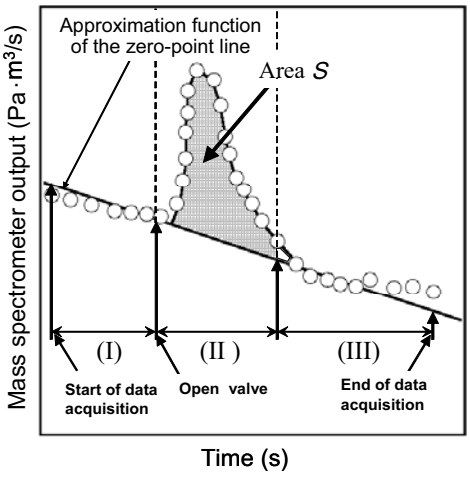

Fig. 13 Transient waveform of mass-spectrometer output at mass number 4.

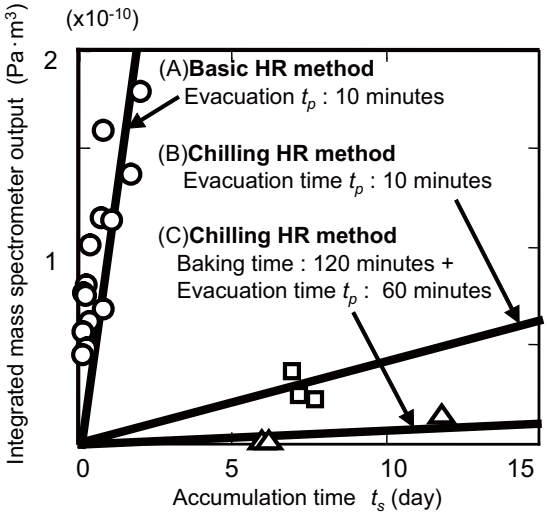

Fig. 15 Integrated mass-spectrometer output as a function of accumulation time.

conventional helium vacuum integration method. The leak-rate resolution was improved by baking and lengthening the evacuation time. The leak-rate resolution of 1×10^{-17} Pa·m^3/s obtained by the chilling HR method with baking (C) is 10^5 times superior to the conventional method. The leak-rate resolutions under different conditions are summarized in **Table 1**. These results indicate that the proposed chilling HR method is useful in developing a vacuum hermetic package. The proposed method is applicable to the development of an automotive angular rate sensor.

5. Conclusion

Three types of elemental technologies useful for the development of a capacitive MEMS sensor were developed. These technologies are extremely deep silicon etching (EDSE) using a compensation mask pattern, a *z*-directional anti-stiction technology using a poly-Si mushroom-shaped structure (pSiMS), and a high-resolution (HR) leak-test method.

The EDSE using the proposed compensation pattern successfully fabricated a 300-μm-thick sense-comb structure without a bridge-shaped silicon residue. The proposed EDSE is useful for the fabrication of complicated and extremely thick structures with different gap widths. Next, the proposed pSiMS with a height of 0.6 μm prevented 2-mm-long beams from *z*-directional sticking. Therefore, this pSiMS improves the reliability of a movable SOI-MEMS structure. In addition, the proposed chilling HR method exhibited a leak-rate resolution of 1×10^{-17} Pa·m^3/s. The results demonstrated that the method is useful in order to develop a vacuum hermetic package for a sensor.

Effectively, these elemental technologies help to develop an automotive MEMS sensor.

Table 1 Leak-rate resolution under different conditions for three test methods.

Conditions	Baking time (min)	Evacuation time t_p (min)	Resolution (Pa·m^3/s)
(A) Basic HR	–	10	1x10^{-15}
(B) Chilling HR	–	10	4x10^{-17}
(C) Chilling HR with baking	120 (at 150°C)	60	1x10^{-17}

Acknowledgements

The authors would like to thank Mr. Hidemi Senda from Toyota Motor Corporation for his valuable suggestions and cooperation during the investigation of the HR package leak test.

References

(1) "Vehicle Stability Control (VSC)", TOYOTA ESQ Communications, <http://www.toyota.com/esq/articles/2010/VSC.html>, (accessed 2012-05-28).
(2) Hynes, A. M., Ashraf, H., Bhardwaj, J. K., Hopkins, J., Johnson, I. and Shepherd, J. N., *Sensors and Actuators A*, Vol.74 (1997), pp.13-17.
(3) Seidel, H., Csepregi, L., Heuberger, A. and Baumgärtel, H., *J. Electrochem. Soc.*, Vol.137 (1990), pp.3612-3625.
(4) Shikida, M., Sato, K., Tokoro, K. and Uchikawa, D., *Sensors and Actuators A*, Vol.80 (2000), pp.179-188.
(5) Tabata, O., Asahi, R., Funabashi, H., Shimaoka, K. and Sugiyama, S., *Sensors and Actuators A*, Vol.34 (1992), pp.51-57.
(6) Yeom, J., Wu, Y. and Shannon, M. A., *Digest Tech. Papers Transducers '03 Conference* (2003), pp.1631-1634.
(7) Kim, J., Park, S., Kwak, D., Ko, H., Carr, W., Buss, J. and Cho, D. D., *Sensors and Actuators A*, Vol.114 (2004), pp.236-243.
(8) Tas, N., Sonnenberg, T., Jansen, H., Legtenberg, R. and Elwenspoek, M., *J. Micromech. Microeng.*, Vol.6 (1996), pp.385-397.
(9) Mastrangelo, C. H. and Hsu, C. H., *J. Microelectromech. Syst.*, Vol.2, No.1 (1993), pp.44-55.
(10) Maenaka, K., Fujita, T., Konishi, Y. and Maeda, M., *Sensors and Actuators A*, Vol.54 (1996), pp.568-573.
(11) JIS (Japanese Industrial Standards) Z 2331:2006, JIS Z 2332:1993, JIS Z 2333:2005, JIS C 0026:2001, JIS C 6701:2007.

Figs. 12-15 and Table 1
Reprinted from Proceedings of the 22nd IEEE International Conference on Micro Electro Mechanical Systems (IEEE MEMS 2009) (2009), pp.737-740, Fujiyoshi, M., Nonomura, Y. and Senda, H., A New High-sensitivity Package-leak Testing Method for MEMS Sensors, © 2009 IEEE.

Sections 2, 3 and 4
Partially reproduced from IEEE International Conference on Micro Electro Mechanical Systems (IEEE MEMS), 25th (2012), 24th (2011) and 22nd (2009), respectively, © IEEE.

Teruhisa Akashi
Research Fields:
- Development of Inertial MEMS Sensors and Mirror Devices
- Elemental Technologies Based on MEMS Fabrication Processes

Academic Societies:
- The Institute of Electrical Engineers of Japan
- The Japan Society for Precision Engineering

Motohiro Fujiyoshi
Research Field:
- Design and Analysis of Micro Inertial Sensor for Control of Automobile

Academic Degree: Dr.Eng.
Academic Societies:
- The Institute of Electrical Engineers of Japan
- IEEE

Award:
- Transducers 2011 Outstanding Paper Award, 2011

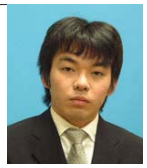

Yoshiyuki Hata
Research Field:
- MEMS Device

Academic Degree: Dr.Sci.
Academic Society:
- The Robotics Society of Japan

Yutaka Nonomura
Research Field:
- Research & Development of MEMS Devices for Automotive Use

Academic Degree: Dr.Eng.
Academic Societies:
- The Magnetic Society of Japan
- The Japan Society of Applied Physics
- The Institute of Electrical Engineers of Japan
- IEEE

Awards:
- R&D100 Award, 1993 and 2001

Hirofumi Funabashi
Research Field:
- Sensors for Automobile and MEMS Technology

Academic Society:
- The Institute of Electrical Engineers of Japan

Yoshiteru Omura
Research Field:
- Structural Analysis and Evaluation of MEMS Sensors and Semiconductor Devices

Academic Society:
- The Institute of Electrical Engineers of Japan

Award:
- R&D100 Award, 1993